International Journal for Multiscale Computational Engineering, 16(4):367–376 (2018)

MODELING PLASTIC DEFORMATION OF NANO/SUBMICRON-SIZED TUNGSTEN PILLARS UNDER COMPRESSION: A COARSE-GRAINED ATOMISTIC APPROACH

Shuozhi Xu

California NanoSystems Institute, University of California, Santa Barbara, California 93106-6105, USA, E-mail: shuozhixu@ucsb.edu

Original Manuscript Submitted: 3/21/2018; Final Draft Received: 8/12/2018

In this work, coarse-grained atomistic simulations via the concurrent atomistic-continuum (CAC) method are performed to investigate compressive deformation of nano-/submicron-sized pillars in body-centered cubic (BCC) tungsten. Two models with different surface roughness are considered. All pillars have the same height-to-diameter aspect ratio of 3, with the diameter ranging from 27.35 to 165.34 nm; as a result, the largest simulation cell contains 291,488 finite elements, compared to otherwise ≈ 687.82 million atoms in an equivalent full atomistic model. Results show that (i) a larger surface roughness leads to a lower yield stress and (ii) the yield stress of pillars with a large surface roughness scales nearly linearly with the diameter while that of pillars with smooth surfaces scales exponentially with the diameter, the latter of which agrees with experiments. The differences in the yield stress between the two models are attributed to their different plastic deformation mechanisms: in the case of large surface roughness, dislocation nucleation is largely localized near the ends of the pillars; and in pillars with smooth surfaces, dislocation avalanches in a more homogeneous manner are observed. This work, which is the first attempt to simulate BCC systems using the CAC method, highlights the significance of the surface roughness in uniaxial deformation of nano-/submicropillars.

KEY WORDS: *concurrent atomistic-continuum method, compression, tungsten, pillar*

1. INTRODUCTION

Extrinsic size effects in metals due to dimensional constraints significantly influence mechanical properties of materials, especially so at the nano and micronscales (Greer et al., 2009; Hammami and Kulkarni, 2014). Examples include small-sized pillars that, distinguished by their diameter D, can be classified into nanopillars ($D \leq 100$ nm), submicropillars (100 nm $< D \leq 1\mu$m), and micropillars ($D > 1$ μm). Plastic deformation of pillars has been extensively studied using experimental (Brinckmann et al., 2008) and modeling (Weinberger and Cai, 2008) approaches, with a focus on the yield/flow stress as a function of the pillar diameter, height-to-diameter aspect ratio, cross-sectional shape, strain rate, temperature, lattice orientations, boundary conditions, etc., in a wide range of metallic materials. For example, the discrete dislocation dynamics (DDD) method, which assumes the motion of dislocations as the only carrier of plasticity, has been applied to simulating nanopillars (Papanikolaou et al., 2017), submicropillars (Cui et al., 2017), and micropillars (El-Awady, 2015). However, besides dislocation slip, processes such as twinning and phase transformation have also been identified as possible plastic deformation mechanisms in nano-/micropillars (Greer and De Hosson, 2011) in both face-centered cubic (FCC) and body-centered cubic (BCC) metallic systems. Even in the same material, the specific dominating mechanism depends on a number of geometric factors and/or loading conditions. Take the BCC Fe nanopillar as an example, Sainath and Choudhary (2016) found that the ⟨100⟩- and ⟨110⟩-oriented nanopillars respectively deform by twinning and dislocation slip under tension, while deform by dislocation slip and twinning, respectively, under compression. In addition, in DDD simulations, the pillar surface must acquire pre-existing dislocation sources, from which dislocations are multiplied. Thus, DDD is limited to

1543–1649/18/$35.00 © 2018 by Begell House, Inc. www.begellhouse.com

cases in which dislocation slip is the dominating plastic deformation mechanism and dislocation sources are known *a priori*.

On the other hand, atomistic simulation methods, such as molecular dynamics (MD), do not rely on any *a priori* assumption regarding the plasticity mechanisms and are thus desirable in exploring deformed pillars. However, MD simulations of submicro-/micropillars are exceedingly expensive—to the author's best knowledge, the largest atomistic pillar models to date contained about 45 million atoms (Gu et al., 2012; Xu et al., 2017a,b), with the maximum $D = 70$ nm (i.e., in the nanopillar regime). Therefore, in this paper, a coarse-grained atomistic approach named the concurrent atomistic-continuum (CAC) method (Chen, 2009; Xiong et al., 2011; Xu et al., 2015) is employed to explore the plastic deformation of nano-/submicron-sized metallic pillars. As a concurrent partitioned-domain multiscale modeling technique, the CAC simulation scheme usually partitions the whole problem into two domains: an atomistic domain and a coarse-grained domain (Xu and Chen, 2018). Unlike most concurrent multiscale materials modeling approaches in the literature [e.g., the quasicontinuum method (Marian and Knap, 2007)], CAC admits a two-way exchange of dislocations between atomistic and coarse-grained domains without adopting adaptive mesh refinement, enabled by the usage of discontinuous finite elements in the latter domain and with the interatomic potential as the only constitutive rule (Xu et al., 2018c).

The theoretical foundation of the CAC method is the atomistic field theory (AFT) (Chen, 2009; Chen and Lee, 2005), which views a crystalline material as a continuous collection of material points (unit cells), within each of which are discrete atoms possessing internal degrees of freedom. With a unified atomistic-continuum integral formulation in both atomistic and coarse-grained domains, AFT employs the interatomic potential as the only constitutive rule. Previously, simulations based on AFT were carried out to investigate deformation of nanopillars with $D < 10$ nm in diamond (Xiong and Chen, 2009a; Xiong et al., 2007), 3C-SiC (Xiong et al., 2007), and MgO (Xiong and Chen, 2009b; Xiong et al., 2008), predicting similar stress-strain curves as MD. However, in all those studies, continuous finite elements were employed in the coarse-grained domain so that only phase transformation, but not dislocation slip or twinning, was reproduced. In this paper, the same problem, (i.e., deformation of pillars) is revisited using CAC simulations equipped with discontinuous finite elements that have the capability to accommodate dislocations besides phase transformation. To showcase the advantage of CAC in extending the accessible length scales, the current work explores nano-/submicropillars with D ranging from 27.35 to 165.34 nm in BCC tungsten (W).

Although CAC has been employed to pursue a series of dislocation-mediated nano-/microscale mechanical problems in FCC metals (Chen et al., 2018; Xiong et al., 2015, 2016; Xu et al., 2016a,b,c,d, 2017c,d), modeling of dislocations in BCC systems using CAC was not conducted because it was believed that dislocation core structures in BCC materials are nonplanar (Ito and Vitek, 2001; Vitek et al., 1970) and would not be accurately captured by the coarse-grained atomistic descriptions in CAC. However, recent density functional theory calculations confirmed that dislocations in most BCC transition metals have a compact nondegenerate core structure (Weinberger et al., 2013b); accordingly, new interatomic potentials have been developed and validated for relevant dislocation cores (Bonny et al., 2014). On the basis of this new knowledge, CAC is expected to well describe the dislocation cores in BCC metals as long as suitable potentials are employed (Chavoshi et al., 2017; Xu and Su, 2018; Xu et al., 2018d). Hence, an attempt is made in this paper to quantify the dislocation-related properties and explore plastic deformation of pillars in a BCC lattice via CAC simulations.

2. MATERIALS AND METHODS

Taper-free single crystalline cylindrical pillars are cut from rectangular prisms with $x[100]$, $y[010]$, and $z[001]$ crystallographic orientations. The central axis of the pillar is along the z direction, with a fixed height-to-diameter aspect ratio of 3 following Gu et al. (2012) while the diameter D is varied from 27.35 to 165.34 nm. Three-dimensional rhombohedral finite elements with faces on $\{110\}$ planes in W are employed. A uniform element size of 2197 atoms per element is chosen, with all simulation cell boundaries assumed to be traction-free. Two models, shown in Fig. 1, are considered: (i) in Model-A, fully coarse-grained models are used with jagged boundaries as a result of the peculiar shape of the rhombohedral elements—accordingly, the pillars have elemental scale surface roughness; and (ii) in Model-B, the jagged boundaries in Model-A are "filled in" by atoms, resulting in pillars with atomic-scale surface roughness. In other words, only a coarse-grained domain is employed in Model-A; whereas, both coarse-grained and

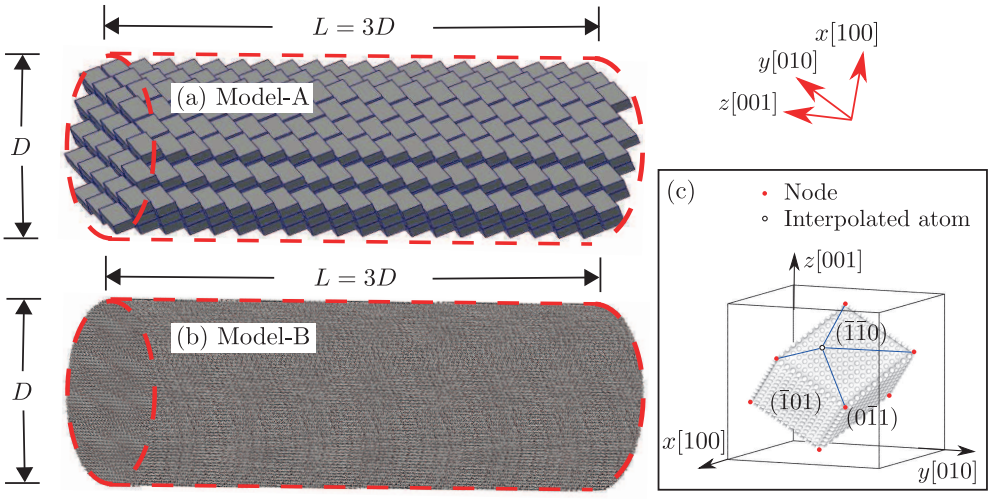

FIG. 1: Two CAC models of pillars in BCC W with $D = 27.35$ nm. In Model-A, the simulation cell consists of only finite elements, with jagged boundaries; in Model-B, atomistic domains are introduced to "fill in" the interstices between boundaries of a cylinder and element boundaries

atomistic domains are adopted in Model-B. As a result, the largest model with $D = 165.34$ nm contains 291,488 finite elements in Model-A and an additional 47.42 million atoms in Model-B, respectively, corresponding to about 640.4 and 687.82 million atoms in equivalent full atomistic simulation cells. Embedded-atom method (EAM) potentials by Marinica et al. (2013) are employed for interatomic interactions, with a lattice parameter $a_0 = 3.14339$ Å. Once the initial models are built, dynamic relaxation with a zero stress tensor and at 10 K is conducted under a NPT ensemble for 50 ps, before the pillars are energy minimized using the conjugate gradient algorithm (Xu et al., 2015). It follows that homogeneous compressive engineering strain with a constant rate of 10^9 s^{-1} and time step of 5 fs is applied along the axial z direction. All CAC simulations are carried out using PyCAC (Xu, 2017; Xu et al., 2018b). Atomistic structures are visualized in OVITO (Stukowski, 2010) with lattice defects identified by the centrosymmetry parameter (CSP) (Kelchner et al., 1998).

3. MODEL VALIDATION

First, following Xu et al. (2015), the newly developed finite element shown in Fig. 1(c) is validated in terms of the interatomic force/energy and generalized stacking fault energy (GSFE). Although $\{111\}$ planes are the primary slip planes in FCC crystals, dislocations in BCC systems can glide on $\{110\}$, $\{112\}$, and $\{123\}$ planes (Weinberger et al., 2013a). However, specifically for W, only dislocation slip on $\{110\}$ planes was observed in uniaxially deformed $\langle 112\rangle$-oriented nanopillars/tubes in MD simulations (Xu and Chavoshi, 2018; Xu et al., 2017a, 2018a) using the same EAM potential (Marinica et al., 2013), plausibly due to the lowest stacking fault energy on $\{110\}$ planes among all three sets of likely slip planes. The kink pair theory proposed by Butt (2007) also predicts that the primary slip planes at relatively low temperatures (< 220 K) are $\{110\}$ planes. On the other hand, the second nearest-neighbor (2NN) element, whose integration points are within 2NN distance from the element surface (Xu et al., 2015), provides a reasonable approximation for interatomic force/energy and the GSFE on a $\{110\}$ plane along a $\langle 111\rangle$ direction in W, as shown in Fig. 2.

In addition, the kink-pair formation during motion of screw dislocations in BCC lattices (Narayanan et al., 2014) is naturally accommodated between discontinuous elements in a way similar to the intrinsic stacking fault in FCC systems. Note that while the coarse-grained domain in CAC does not naively permit extrinsic stacking faults and twins (Xu et al., 2017e), no twining was reported in uniaxial compression of $\langle 100\rangle$-oriented W submicropillars (Kim et al., 2010) and micropillars (Schneider et al., 2009b, 2011) in experiments. Wang et al. (2015) found that the plasticity of a $\langle 100\rangle$-oriented nanopillar is dominated by twinning under tensile deformation, but the case under compressive

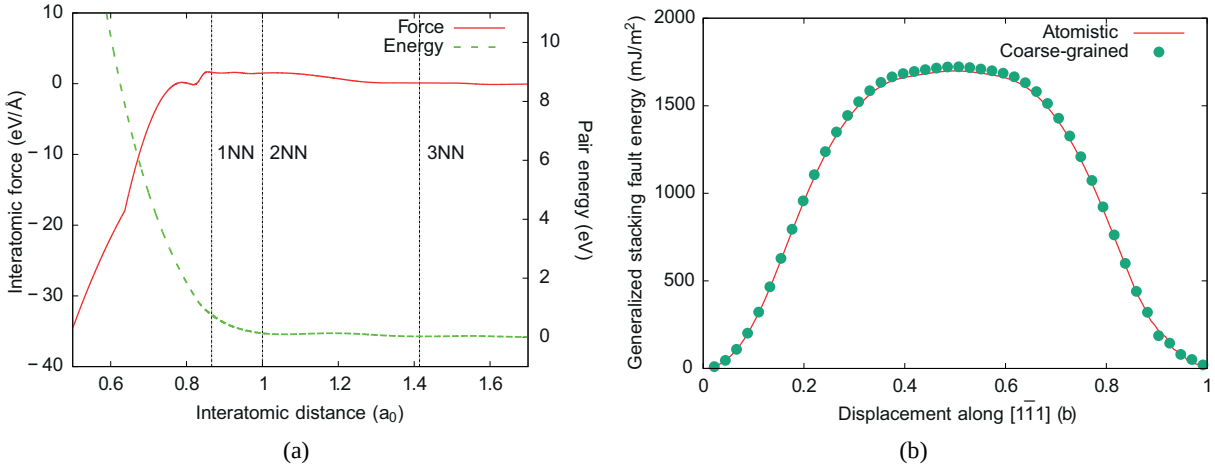

(a) (b)

FIG. 2: Certain quantities for W calculated using the EAM potential (Marinica et al., 2013): (a) The interatomic force and pair energy with respect to the interatomic distance. Changes in the force and energy are negligible when the distance is beyond the 2NN distance. Note that the host electron density is assumed constant; thus, only the force contribution from the pair potential is shown here. (b) Relaxed GSFE on a $\{111\}$ plane along the $[1\bar{1}1]$ direction; b is the magnitude of the Burgers vector of a full dislocation $\mathbf{b} = (a_0/2)\langle 111\rangle$

deformation remained experimentally unexplored, to the best of the author's knowledge. Thus, equivalent MD simulations are conducted using LAMMPS (Plimpton, 1995) for the nanopillars with $D = 27.35$ nm. Figure 3 shows that CAC and MD simulations predict similar stress-strain responses for both models, with CAC having larger amplitudes of postyielding discrete strain bursts than MD, as a result of the linear shape functions employed in the coarse-grained domain in CAC (Xiong et al., 2011). Only dislocations on $\{110\}$ planes, but no twinning, are observed in MD simulations. Therefore, it is anticipated that the finite element illustrated in Fig. 1(c) can reasonably well replicate essential aspects of dislocation-mediated plastic deformation in W nano-/submicropillars.

4. RESULTS AND DISCUSSION

In both models, upon yielding, dislocations are nucleated from the free surfaces near the ends of the pillars, as shown in Fig. 4. For the same pillar diameter D, Model-A has a much lower yield stress than Model-B, due to the larger surface roughness and accompanying higher local stress concentration in the former. At larger strains, dislocations start to nucleate from the free surfaces away from the ends of the pillars and glide on $\{110\}$ planes. Dislocation

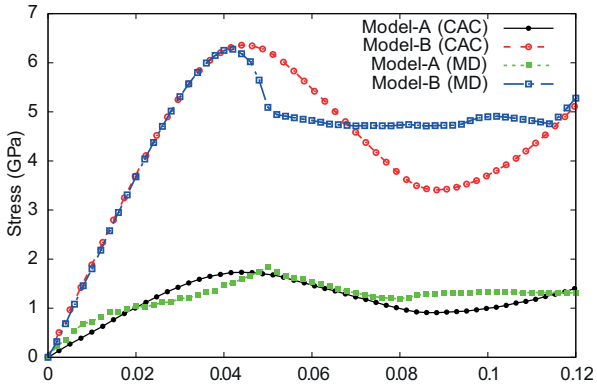

FIG. 3: Stress-strain curves obtained from CAC and MD simulations for Model-A and Model-B with $D = 27.35$ nm

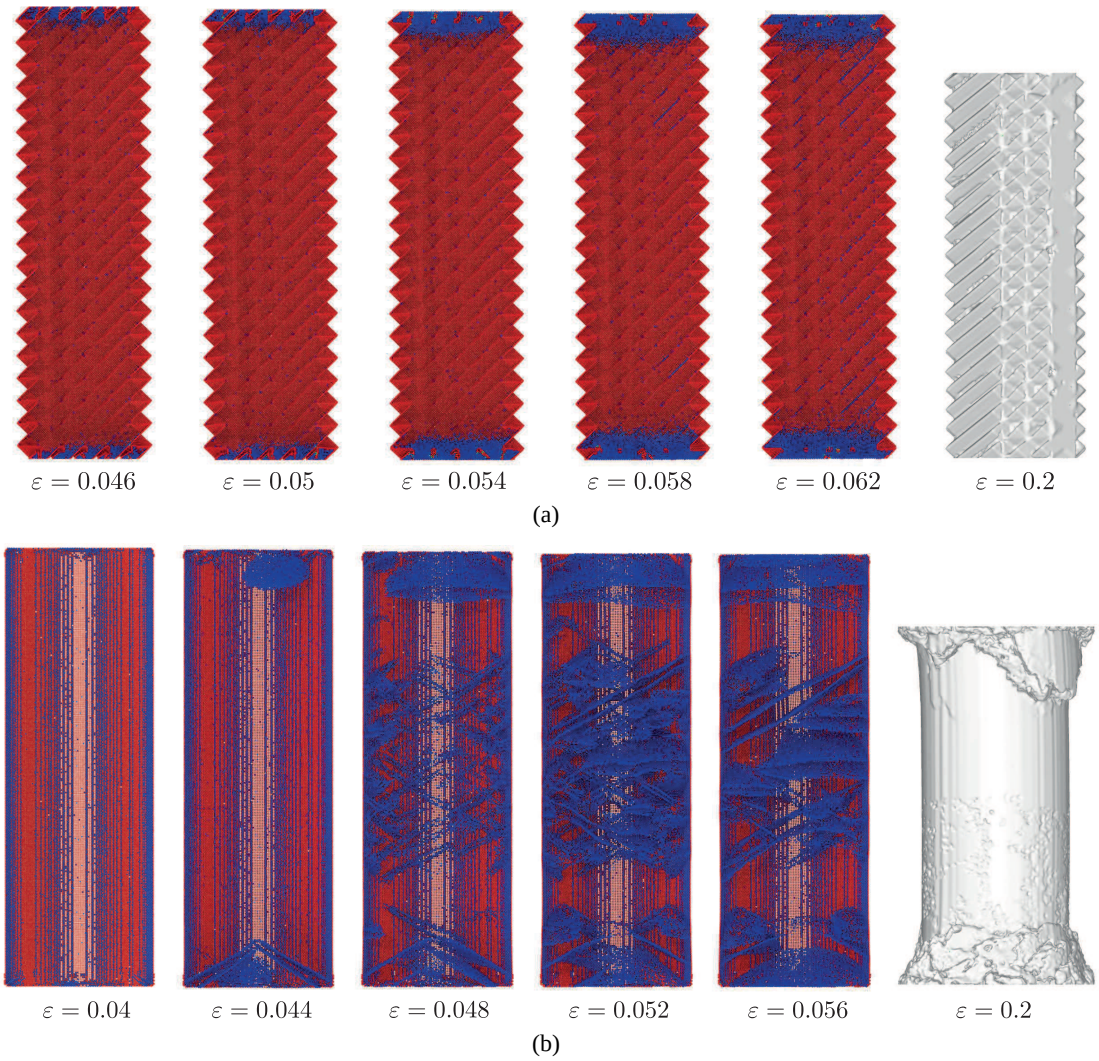

FIG. 4: Snapshots of configurations in (a) Model-A and (b) Model-B with $D = 55.01$ nm projected on the y-z plane. In the first five snapshots of each row, atoms are colored by CSP (Kelchner et al., 1998) between 0 and 2; those with a CSP smaller than 0.05 are deleted. In the last snapshot of each row, only surface morphology is shown

avalanches are observed in Model-B but not in Model-A, as a result of the much higher stress level in the former. At the largest strain of 0.2, pronounced localized bulging is observed at both ends of the pillars in Model-B; however, the pillars approximately maintain their original surface morphology in Model-A, indicating that the larger surface roughness leads to more resilient pillar structures under compression.

Stress-strain curves for the two models with varying pillar diameter D are plotted in Fig. 5. The yield stresses σ_Y, taken at the initiation of dislocations, are summarized in Fig. 6. Since previous experiments have identified that the pillar strength scales with the diameter in a power law fashion (Greer and De Hosson, 2011), a simple equation is fit to σ_Y, i.e.,

$$\sigma_Y(D) = \sigma_0 + kD^n \tag{1}$$

where σ_0, k, and n are parameters to be fit. It is found that n is 0.96 and -1.48 for Model-A and Model-B, respectively. In other words, σ_Y increases with D nearly linearly for Model-A while decreases with D exponentially for Model-B.

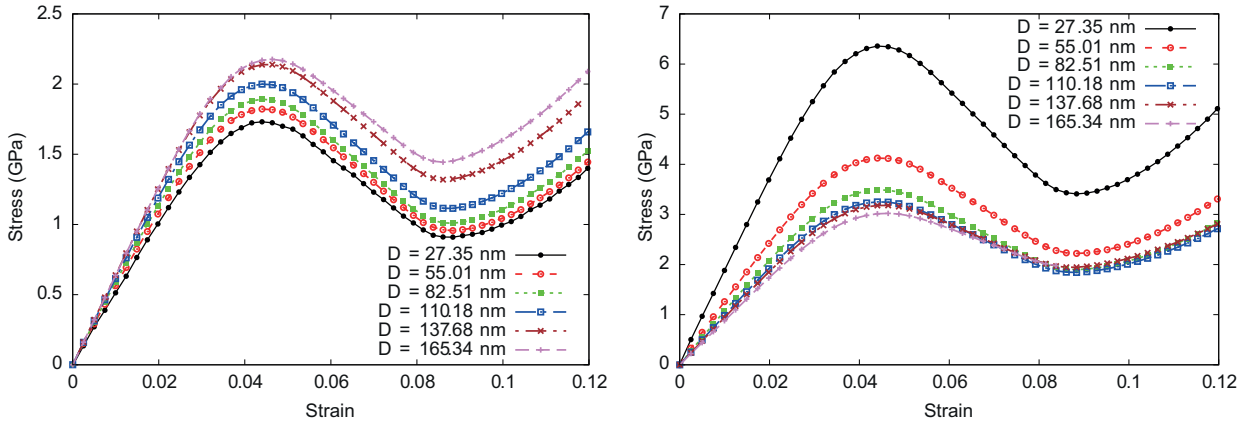

FIG. 5: Stress-strain curves for (a) Model-A and (b) Model-B as a function of pillar diameter D

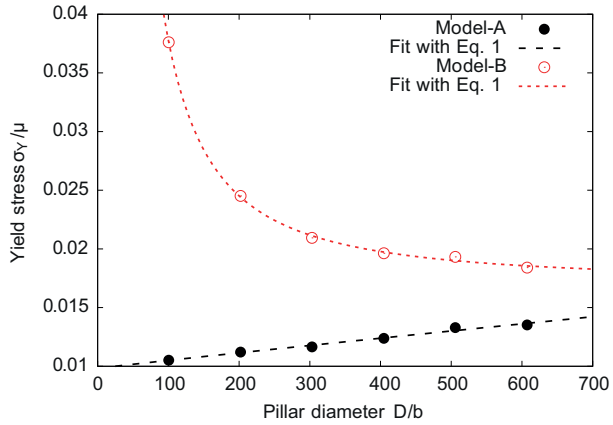

FIG. 6: Yield stresses σ_Y for Model-A and Model-B as a function of pillar diameter D. $\mu = 161$ GPa is the shear modulus for the $\{110\}\langle 111\rangle$ slip system

The differences in n between the two models are results of their different deformation mechanisms. In Model-A, the yielding is controlled by dislocation nucleation from the sharp edges/corners formed by jagged elements at the free surfaces at relatively low compressive stress levels, a highly localized phenomenon having little size dependence; and in Model-B, the yielding is exhibited by rapid dislocation avalanches nucleated from the pillar surfaces at relatively high stress levels, which promotes the formation of dislocation junctions and single-arm Frank-Read sources that are more difficult to activate in smaller pillars (Brinckmann et al., 2008). Note that the two fit curves in Fig. 6 are extrapolated to intersect at $D \approx 340$ nm, for which the surface roughness, $0.006D$, is negligible.

In experimentally compressed $\langle 100\rangle$-oriented submicron W pillars having small surface roughness, i.e., more like Model-B than Model-A, (i) localized bulging at the apex of the pillars was reported, as a result of a more avalanche dominated behavior caused by the activation of only a few slip systems, and (ii) the power law slope n of the flow stress is -0.44 (Kim et al., 2010) or -0.33 (Torrents Abad et al., 2016) at room temperature. Although there are no experimental data in the literature with which the pillars considered here can be directly compared, the power law scaling identified in this work qualitatively agrees with that found by experiments. Note that in experiments, a higher loading rate increases the flow stress and the power law slope (Schneider et al., 2009a). Thus, the higher n predicted in this work for Model-B may be attributed in part to the much higher strain rates (10^9 s^{-1}) employed in CAC simulations compared to those (10^{-7} to 10^{-1} s^{-1}) in experiments.

5. CONCLUSIONS

In this work, large-scale CAC simulations are conducted to investigate plastic deformation of nano-/submicron-sized W pillars under compression. The pillar diameter D varies from 27.35 to 165.34 nm. Two models are considered: Model-A is fully coarse-grained with large surface roughness, and Model-B is partly coarse-grained and partly atomistic with smooth surfaces. For pillars with small D, CAC simulation results are benchmarked against MD for validation. It is found that (i) for the same D, Model-A has a much lower yield stress than Model-B, and (ii) the yield stress scales with D nearly linearly for Model-A but exponentially for Model-B, the latter of which agrees with experiments. The differences between the two models are attributed to their different plastic deformation mechanisms, i.e., localized dislocation nucleation at a low stress level in Model-A and dislocation avalanches at a high stress level in Model-B. As the first attempt to simulate BCC systems using the CAC method, this work highlights the significance of the surface roughness in uniaxial deformation of nano-/submicropillars in BCC W. Future work will consider the effects of taper (Fei et al., 2012), the height-to-diameter aspect ratio (Milne et al., 2011), and the finite element shape (Xu, 2016). Work is also underway to implement new finite elements for more complex systems with hexagonal close-packed and diamond cubic crystal structures into PyCAC.

ACKNOWLEDGMENTS

The work was supported in part by the Elings Prize Fellowship in Science offered by the California NanoSystems Institute (CNSI) on the UC Santa Barbara campus. The author also acknowledges support from the Center for Scientific Computing from the CNSI, MRL: an NSF MRSEC (Grant No. DMR-1121053). This work used the Extreme Science and Engineering Discovery Environment (XSEDE), which is supported by National Science Foundation Grant No. ACI-1053575.

REFERENCES

Bonny, G., Terentyev, D., Bakaev, A., Grigorev, P., and Neck, D.V., Many-Body Central Force Potentials for Tungsten, *Model. Simul. Mater. Sci. Eng.*, vol. **22**, no. 5, p. 053001, from http://stacks.iop.org/0965-0393/22/i=5/a=053001, 2014.

Brinckmann, S., Kim, J.Y., and Greer, J.R., Fundamental Differences in Mechanical Behavior between Two Types of Crystals at the Nanoscale, *Phys. Rev. Lett.*, vol. **100**, no. 15, p. 155502, 2008. DOI: 10.1103/PhysRevLett.100.155502

Butt, M.Z., Kinetics of Flow Stress in Crystals with High Intrinsic Lattice Friction, *Philos. Mag.*, vol. **87**, no. 24, pp. 3595–3614, 2007. DOI: 10.1080/14786430701370850

Chavoshi, S.Z., Xu, S., and Goel, S., Addressing the Discrepancy of Finding the Equilibrium Melting Point of Silicon using Molecular Dynamics Simulations, *Proc. R. Soc. A*, vol. **473**, no. 2202, p. 20170084, from http://rspa.royalsocietypublishing.org/content/473/2202/20170084, 2017.

Chen, H., Xu, S., Li, W., Ji, R., Phan, T., and Xiong, L., A Spatial Decomposition Parallel Algorithm for a Concurrent Atomistic-Continuum Simulator and Its Preliminary Applications, *Comput. Mater. Sci.*, vol. **144**, pp. 1–10, from https://www.sciencedirect.com/science/article/pii/S0927025617306845, 2018.

Chen, Y., Reformulation of Microscopic Balance Equations for Multiscale Materials Modeling, *J. Chem. Phys.*, vol. **130**, no. 13, p. 134706, from http://jcp.aip.org/resource/1/jcpsa6/v130/i13/p134706_s1, 2009.

Chen, Y. and Lee, J., Atomistic Formulation of a Multiscale Field Theory for Nano/Micro Solids, *Philos. Mag.*, vol. **85**, nos. 33-35, pp. 4095–4126, 2005. DOI: 10.1080/14786430500362595

Cui, Y., Po, G., and Ghoniem, N., Influence of Loading Control on Strain Bursts and Dislocation Avalanches at the Nanometer and Micrometer Scale, *Phys. Rev. B*, vol. **95**, no. 6, p. 064103, 2017. DOI: 10.1103/PhysRevB.95.064103

El-Awady, J.A., Unravelling the Physics of Size-Dependent Dislocation-Mediated Plasticity, *Nat. Comm.*, vol. **6**, p. 5926, from http://www.nature.com/ncomms/2015/150106/ncomms6926/full/ncomms6926.html#ref22, 2015.

Fei, H., Abraham, A., Chawla, N., and Jiang, H., Evaluation of Micro-Pillar Compression Tests for Accurate Determination of Elastic-Plastic Constitutive Relations, *J. Appl. Mech*, vol. **79**, no. 6, p. 061011, 2012. DOI: 10.1115/1.4006767

Greer, J.R. and De Hosson, J.T.M., Plasticity in Small-Sized Metallic Systems: Intrinsic Versus Extrinsic Size Effect, *Prog. Mater. Sci.*, vol. **56**, no. 6, pp. 654–724, from http://www.sciencedirect.com/science/article/pii/S0079642511000065, 2011.

Greer, J.R., Kim, J.Y., and Burek, M.J., The *In-Situ* Mechanical Testing of Nanoscale Single-Crystalline Nanopillars, *JOM*, vol. **61**, no. 12, pp. 19–25, from http://link.springer.com/article/10.1007/s11837-009-0174-8, 2009.

Gu, X.W., Loynachan, C.N., Wu, Z., Zhang, Y.W., Srolovitz, D.J., and Greer, J.R., Size-Dependent Deformation of Nanocrystalline Pt Nanopillars, *Nano Lett.*, vol. **12**, no. 12, pp. 6385–6392, 2012. DOI: 10.1021/nl3036993

Hammami, F. and Kulkarni, Y., Size Effects in Twinned Nanopillars, *J. Appl. Phys.*, vol. **116**, no. 3, p. 033512, 2014. DOI: 10.1063/1.4890541

Ito, K. and Vitek, V., Atomistic Study of Non-Schmid Effects in the Plastic Yielding of BCC Metals, *Philos. Mag. A*, vol. **81**, no. 5, pp. 1387–1407, 2001. DOI: 10.1080/01418610108214447

Kelchner, C.L., Plimpton, S.J., and Hamilton, J.C., Dislocation Nucleation and Defect Structure during Surface Indentation, *Phys. Rev. B*, vol. **58**, no. 17, pp. 11085–11088, 1998. DOI: 10.1103/PhysRevB.58.11085

Kim, J.Y., Jang, D., and Greer, J.R., Tensile and Compressive Behavior of Tungsten, Molybdenum, Tantalum and Niobium at the Nanoscale, *Acta Mater.*, vol. **58**, no. 7, pp. 2355–2363, from http://www.sciencedirect.com/science/article/pii/S1359645409008647, 2010.

Marian, J. and Knap, J., Breakdown of Self-Similar Hardening Behavior in Au Nanopillar Microplasticity, *Int. J. Multiscale Comput. Eng.*, vol. **5**, nos. 3-4, pp. 287–294, from http://www.dl.begellhouse.com/journals/61fd1b191cf7e96f,3cf3b25417fa966d,65fbfc9570d20cbe.html, 2007.

Marinica, M.C., Ventelon, L., Gilbert, M.R., Proville, L., Dudarev, S.L., Marian, J., Bencteux, G., and Willaime, F., Interatomic Potentials for Modelling Radiation Defects and Dislocations in Tungsten, *J. Phys.: Condens. Matter*, vol. **25**, no. 39, p. 395502, from http://stacks.iop.org/0953-8984/25/i=39/a=395502, 2013.

Milne, R.J., Lockwood, A.J., and Inkson, B.J., Size-Dependent Deformation Mechanisms of Al Nanopillars, *J. Phys. D: Appl. Phys.*, vol. **44**, no. 48, p. 485301, from http://iopscience.iop.org/0022-3727/44/48/485301, 2011.

Narayanan, S., McDowell, D.L., and Zhu, T., Crystal Plasticity Model for BCC Iron Atomistically Informed by Kinetics of Correlated Kinkpair Nucleation on Screw Dislocation, *J. Mech. Phys. Solids*, vol. **65**, pp. 54–68, from http://www.sciencedirect.com/science/article/pii/S0022509614000143, 2014.

Papanikolaou, S., Song, H., and Van der Giessen, E., Obstacles and Sources in Dislocation Dynamics: Strengthening and Statistics of Abrupt Plastic Events in Nanopillar Compression, *J. Mech. Phys. Solids*, vol. **102**, pp. 17–29, from http://www.sciencedirect.com/science/article/pii/S0022509616304112, 2017.

Plimpton, S., Fast Parallel Algorithms for Short-Range Molecular Dynamics, *J. Comput. Phys.*, vol. **117**, no. 1, pp. 1–19, from http://www.sciencedirect.com/science/article/pii/S002199918571039X, 1995.

Sainath, G. and Choudhary, B.K., Deformation Behaviour of Body Centered Cubic Iron Nanopillars Containing Coherent Twin Boundaries, *Philos. Mag.*, vol. **96**, nos. 32-34, pp. 3502–3523, 2016. DOI: 10.1080/14786435.2016.1240377

Schneider, A.S., Clark, B.G., Frick, C.P., Gruber, P.A., and Arzt, E., Effect of Orientation and Loading Rate on Compression Behavior of Small-Scale Mo Pillars, *Mater. Sci. Eng. A*, vol. **508**, no. 1, pp. 241–246, from http://www.sciencedirect.com/science/article/pii/S0921509309000227, 2009a.

Schneider, A.S., Kaufmann, D., Clark, B.G., Frick, C.P., Gruber, P.A., Mönig, R., Kraft, O., and Arzt, E., Correlation between Critical Temperature and Strength of Small-Scale BCC Pillars, *Phys. Rev. Lett.*, vol. **103**, no. 10, p. 105501, 2009b. DOI: 10.1103/PhysRevLett.103.105501

Schneider, A.S., Frick, C.P., Clark, B.G., Gruber, P.A., and Arzt, E., Influence of Orientation on the Size Effect in BCC Pillars with Different Critical Temperatures, *Mater. Sci. Eng. A*, vol. **528**, no. 3, pp. 1540–1547, from http://www.sciencedirect.com/science/article/pii/S0921509310012517, 2011.

Stukowski, A., Visualization and Analysis of Atomistic Simulation Data with OVITO—The Open Visualization Tool, *Model. Simul. Mater. Sci. Eng.*, vol. **18**, no. 1, p. 015012, from http://iopscience.iop.org/0965-0393/18/1/015012, 2010.

Torrents Abad, O., Wheeler, J.M., Michler, J., Schneider, A.S., and Arzt, E., Temperature-Dependent Size Effects on the Strength of Ta and W Micropillars, *Acta Mater.*, vol. **103**, pp. 483–494, from http://www.sciencedirect.com/science/article/pii/S1359645415300173, 2016.

Vitek, V., Perrin, R.C., and Bowen, D.K., The Core Structure of 1/2(111) Screw Dislocations in BCC Crystals, *Philos. Mag. A*, vol. **21**, no. 173, pp. 1049–1073, 1970.

Wang, J., Zeng, Z., Weinberger, C.R., Zhang, Z., Zhu, T., and Mao, S.X., *In Situ* Atomic-Scale Observation of Twinning-Dominated Deformation in Nanoscale Body-Centred Cubic Tungsten, *Nat. Mater.*, vol. **14**, no. 6, pp. 594–600, from http://www.nature.com/nmat/journal/v14/n6/full/nmat4228.html, 2015.

Weinberger, C.R. and Cai, W., Surface-Controlled Dislocation Multiplication in Metal Micropillars, *Proc. Natl. Acad. Sci. USA*, vol. **105**, no. 38, pp. 14304–14307, from http://www.pnas.org/content/105/38/14304, 2008.

Weinberger, C.R., Boyce, B.L., and Battaile, C.C., Slip Planes in BCC Transition Metals, *Int. Mater. Rev.*, vol. **58**, no. 5, pp. 296–314, 2013a. DOI: 10.1179/1743280412Y.0000000015

Weinberger, C.R., Tucker, G.J., and Foiles, S.M., Peierls Potential of Screw Dislocations in BCC Transition Metals: Predictions from Density Functional Theory, *Phys. Rev. B*, vol. **87**, no. 5, p. 054114, 2013b. DOI: 10.1103/PhysRevB.87.054114

Xiong, L. and Chen, Y., Coarse-Grained Simulations of Single-Crystal Silicon, *Model. Simul. Mater. Sci. Eng.*, vol. **17**, no. 3, p. 035002, from http://stacks.iop.org/0965-0393/17/i=3/a=035002?key=crossref.3408a55064c39876fd5f10e1fecc2bf9, 2009a.

Xiong, L. and Chen, Y., Multiscale Modeling and Simulation of Single-Crystal MgO through an Atomistic Field Theory, *Int. J. Solids Struc.*, vol. **46**, no. 6, pp. 1448–1455, from http://www.sciencedirect.com/science/article/pii/S0020768308004861, 2009b.

Xiong, L., Chen, Y., and Lee, J.D., Atomistic Simulation of Mechanical Properties of Diamond and Silicon Carbide by a Field Theory, *Model. Simul. Mater. Sci. Eng.*, vol. **15**, no. 5, pp. 535–551, from http://stacks.iop.org/0965-0393/15/i=5/a=011?key=crossref.d65b78699253f747ebc520b67c44afa3, 2007.

Xiong, L., Chen, Y., and Lee, J., Simulation of Dislocation Nucleation and Motion in Single Crystal Magnesium Oxide by a Field Theory, *Computational Materials Science*, vol. **42**, no. 1, pp. 168–177, from http://www.sciencedirect.com/science/article/pii/S092702560700184X, 2008.

Xiong, L., Tucker, G., McDowell, D.L., and Chen, Y., Coarse-Grained Atomistic Simulation of Dislocations, *J. Mech. Phys. Solids*, vol. **59**, no. 2, pp. 160–177, from http://www.sciencedirect.com/science/article/pii/S0022509610002395, 2011.

Xiong, L., Xu, S., McDowell, D.L., and Chen, Y., Concurrent Atomistic-Continuum Simulations of Dislocation-Void Interactions in FCC Crystals, *Int. J. Plast.*, vol. **65**, pp. 33–42, from http://www.sciencedirect.com/science/article/pii/S0749641914001508, 2015.

Xiong, L., Rigelesaiyin, J., Chen, X., Xu, S., McDowell, D.L., and Chen, Y., Coarse-Grained Elastodynamics of Fast Moving Dislocations, *Acta Mater.*, vol. **104**, pp. 143–155, from http://www.sciencedirect.com/science/article/pii/S1359645415300884, 2016.

Xu, S., The Concurrent Atomistic-Continuum Method: Advancements and Applications in Plasticity of Face-Centered Cubic Metals, PhD thesis, Georgia Institute of Technology, 2016.

Xu, S., *PyCAC User's Manual*, accessed August 14, 2018, from http://www.pycac.org/, 2017.

Xu, S. and Chavoshi, S.Z., Uniaxial Deformation of Nanotwinned Nanotubes in Body-Centered Cubic Tungsten, *Curr. Appl. Phys.*, vol. **18**, no. 1, pp. 114–121, from http://www.sciencedirect.com/science/article/pii/S1567173917302729, 2018.

Xu, S. and Chen, X., Modeling Dislocations and Heat Conduction in Crystalline Materials: Atomistic/Continuum Coupling Approaches, *Int. Mater. Rev.*, 2018 (in press). DOI: 10.1080/09506608.2018.1486358

Xu, S. and Su, Y., Dislocation Nucleation from Symmetric Tilt Grain Boundaries in Body-Centered Cubic Vanadium, *Phys. Lett. A*, vol. **382**, no. 17, pp. 1185–1189, from http://www.sciencedirect.com/science/article/pii/S0375960118302287, 2018.

Xu, S., Che, R., Xiong, L., Chen, Y., and McDowell, D.L., A Quasistatic Implementation of the Concurrent Atomistic-Continuum Method for FCC Crystals, *Int. J. Plast.*, vol. **72**, pp. 91–126, from http://www.sciencedirect.com/science/article/pii/S0749641915000777, 2015.

Xu, S., Xiong, L., Chen, Y., and McDowell, D.L., An Analysis of Key Characteristics of the Frank-Read Source Process in FCC Metals, *J. Mech. Phys. Solids*, vol. **96**, pp. 460–476, from http://www.sciencedirect.com/science/article/pii/S0022509616301016, 2016a.

Xu, S., Xiong, L., Chen, Y., and McDowell, D.L., Edge Dislocations Bowing out from a Row of Collinear Obstacles in Al, *Scr. Mater.*, vol. **123**, pp. 135–139, from http://www.sciencedirect.com/science/article/pii/S135964621630272X, 2016b.

Xu, S., Xiong, L., Chen, Y., and McDowell, D.L., Sequential Slip Transfer of Mixed-Character Dislocations Across $\Sigma 3$ Coherent Twin Boundary in FCC Metals: A Concurrent Atomistic-Continuum Study, *NPJ Comput. Mater.*, vol. **2**, p. 15016, from http://www.nature.com/articles/npjcompumats201516, 2016c.

Xu, S., Xiong, L., Deng, Q., and McDowell, D.L., Mesh Refinement Schemes for the Concurrent Atomistic-Continuum Method, *Int. J. Solids Struct.*, vol. **90**, pp. 144–152, from http://www.sciencedirect.com/science/article/pii/S0020768316300154, 2016d.

Xu, S., Startt, J.K., Payne, T.G., Deo, C.S., and McDowell, D.L., Size-Dependent Plastic Deformation of Twinned Nanopillars in Body-Centered Cubic Tungsten, *J. Appl. Phys.*, vol. **121**, no. 17, p. 175101, 2017a. DOI: 10.1063/1.4982754

Xu, S., Su, Y., Chen, D., and Li, L., An Atomistic Study of the Deformation Behavior of Tungsten Nanowires, *Appl. Phys. A*, vol. **123**, no. 12, p. 788, from https://link.springer.com/article/10.1007/s00339-017-1414-3, 2017b.

Xu, S., Xiong, L., Chen, Y., and McDowell, D.L., Comparing EAM Potentials to Model Slip Transfer of Sequential Mixed Character Dislocations Across Two Symmetric Tilt Grain Boundaries in Ni, *JOM*, vol. **69**, no. 5, pp. 814–821, from https://link.springer.com/article/10.1007/s11837-017-2302-1, 2017c.

Xu, S., Xiong, L., Chen, Y., and McDowell, D.L., Shear Stress- and Line Length-Dependent Screw Dislocation Cross-Slip in FCC Ni, *Acta Mater.*, vol. **122**, pp. 412–419, from http://www.sciencedirect.com/science/article/pii/S1359645416307601, 2017d.

Xu, S., Xiong, L., Chen, Y., and McDowell, D.L., Validation of the Concurrent Atomistic-Continuum Method on Screw Dislocation/Stacking Fault Interactions, *Crystals*, vol. **7**, no. 5, p. 120, from http://www.mdpi.com/2073-4352/7/5/120, 2017e.

Xu, S., Chavoshi, S.Z., and Su, Y., Deformation Mechanisms in Nanotwinned Tungsten Nanopillars: Effects of Coherent Twin Boundary Spacing, *Phys. Status Solidi RRL*, vol. **12**, no. 3, p. 1700399, 2018a. DOI: 10.1002/pssr.201700399

Xu, S., Payne, T.G., Chen, H., Liu, Y., Xiong, L., Chen, Y., and McDowell, D.L., PyCAC: The Concurrent Atomistic-Continuum Simulation Environment, *J. Mater. Res.*, vol. **33**, no. 7, pp. 857–871, from https://www.cambridge.org/core/journals/journal-of-materials-research/article/pycac-the-concurrent-atomisticcontinuum-simulation-environment/E664F7A8C0AD8DD1673BE2BDE592D0AA, 2018b.

Xu, S., Rigelesaiyin, J., Xiong, L., Chen, Y., and McDowell, D.L., Generalized Continua Concepts in Coarse-Graining Atomistic Simulations, *Generalized Models and Non-classical Approaches in Complex Materials 2*, Advanced Structured Materials, H. Altenbach, J. Pouget, M. Rousseau, B. Collet, and T. Michelitsch, Eds., Cham, Switzerland: Springer, pp. 237–260, from https://link.springer.com/chapter/10.1007/978-3-319-77504-3_12, 2018c.

Xu, S., Su, Y., and Chavoshi, S.Z., Deformation of Periodic Nanovoid Structures in Mg Single Crystals, *Mater. Res. Express*, vol. **5**, no. 1, p. 016523, from http://stacks.iop.org/2053-1591/5/i=1/a=016523, 2018d.